

## THERMAL ANALYSIS STUDIES OF THE DOLOMITE–FERROAN DOLOMITE–ANKERITE SERIES. II. DECOMPOSITION MECHANISM IN FLOWING CO<sub>2</sub> ATMOSPHERE

A.E. MILODOWSKI and D.J. MORGAN

*British Geological Survey, Keyworth, Nottingham, NG12 5GG (Gt. Britain)*

S.St.J. WARNE

*Department of Geology, The University of Newcastle, N.S.W. 2308 (Australia)*

(Received 3 January 1989)

### ABSTRACT

Ankerites and ferroan dolomites [Ca(Mg,Fe)(CO<sub>3</sub>)<sub>2</sub>] dissociate in three stages to give characteristic three-endothermic-peaked DTA curves which correspond to three weight loss steps on TG curves. Pure dolomite decomposes in only two steps. The definition of these phenomena is greatly enhanced by determination in flowing CO<sub>2</sub>. During this investigation a series of well-characterized minerals covering the dolomite–ferroan dolomite–ankerite series was studied using TG–DTG, DTA–EGA, TM and continuous heating X-ray powder photography (“continuous XRD”), backed up by X-ray diffractometry of products cooled from intermediate temperatures (“static” XRD). Limited Mössbauer spectroscopic determinations (reported in detail elsewhere) were also made on intermediate products.

The first stage of the thermal decomposition of dolomite results in the formation of Mg-calcite ((CaMg)CO<sub>3</sub>) and periclase (MgO), with the liberation of CO<sub>2</sub>. In the cases of ankerite and ferroan dolomite, the initial reaction is similar except that a ferroan periclase or magnesian wustite ((Mg,Fe)O) is produced respectively. However, this phase is rapidly oxidized by CO<sub>2</sub> to magnesioferrite (MgFe<sub>2</sub>O<sub>4</sub>). A ferrous spinel (Fe<sub>3</sub>O<sub>4</sub>–MgFe<sub>2</sub>O<sub>4</sub> solid solution) may also be formed as an unstable transient intermediate compound during this oxidation, depending on experimental conditions. As a result, CO is liberated by reduction of CO<sub>2</sub>. The second decomposition step arises out of a solid-state reaction between calcite and magnesioferrite to produce dicalcium ferrite (2CaO·Fe<sub>2</sub>O<sub>3</sub>) and periclase with the evolution of CO<sub>2</sub>. The remaining unreacted calcium carbonate dissociates to CaO and CO<sub>2</sub> in the third decomposition step.

### INTRODUCTION

The dolomite–ferroan dolomite–ankerite series has the general formula AB(CO<sub>3</sub>)<sub>2</sub> where A = Ca<sup>2+</sup> and B = Mg<sup>2+</sup>, Fe<sup>2+</sup>. Ferrous iron substitutes for Mg<sup>2+</sup> in the dolomite (CaMg(CO<sub>3</sub>)<sub>2</sub>) structure and there is complete solid solution from end-member dolomite to approximately 70 mol% CaFe(CO<sub>3</sub>)<sub>2</sub> [1,2]. End-member CaFe(CO<sub>3</sub>)<sub>2</sub> is unknown in nature [3].

Minor amounts of  $\text{Ca}^{2+}$  and often significant amounts of  $\text{Mn}^{2+}$  also substitute for  $\text{Mg}^{2+}$  in some dolomites and ankerites [3]. Members of the dolomite–ferroan dolomite–ankerite series have widespread geological occurrence and significance and are also of industrial importance, either as raw materials or as contaminants in other raw materials.

Minerals from the dolomite end of the series are widely used as raw materials in the chemical, ceramic, refractory, glass, insulation, agricultural, building and roadstone industries. Variations in dolomite–ankerite composition may have petrogenetic significance with respect to associated hydrothermal ore deposits [4] or give valuable information on depositional or diagenetic environments.

The presence of dolomite–ankerite minerals in coals or oil shales has important implications with respect to coal beneficiation, enthalpy, ash fusion temperatures, boiler-tube deposits, corrosion and coke production. Calcined dolomite may be used as a scrubber to remove  $\text{SO}_2$  from flue gases during the combustion of fossil fuels. The thermal decomposition characteristics of dolomites and ankerites may also be important during the extraction of ore minerals from carbonate gangue [5].

The actual composition of the dolomite used industrially is of considerable importance, high Fe contents generally being considered deleterious. Therefore it is necessary to have a reliable method for evaluating these minerals and placing them in the series  $[\text{Ca}(\text{Fe},\text{Mg})(\text{CO}_3)_2]$ . Previous methods have involved X-ray diffraction (XRD) [6,7], differential thermal analysis (DTA) in static air [8], differential staining [9] and infrared (IR) spectroscopy [10]. More recently, in part I of this series of investigations [11], DTA in a flowing  $\text{CO}_2$  atmosphere has been applied to the determination of the Fe content of dolomites and ankerites.

The precise nature of the decomposition reactions and reaction products of these minerals has been the subject of much debate [12–17]. This paper attempts to clarify the understanding of the reactions involved. This is a necessary prerequisite before more quantitative TG techniques can be applied to the evaluation of ankerites and dolomites. The TG evaluation of the dolomite–ferroan dolomite–ankerite series will be presented in a subsequent paper [18].

## EXPERIMENTAL

A series of minerals spanning compositions from end-member dolomite to approximately 60 mol%  $\text{CaFe}(\text{CO}_3)_2$  was assembled and chemically characterized. Chemical analyses, structural formulae and location details of representative examples from this series are given in Table 1.

Samples were freshly crushed by hand to pass a 240 mesh BSS sieve (63  $\mu\text{m}$ ) and checked for purity by X-ray diffraction (XRD) and infrared

TABLE 1

Chemical analyses and structural formulae of minerals of the dolomite-ferroan dolomite-ankerite series ( $\text{CO}_2$  calculated on the basis of  $\text{M}^{2+} \text{CO}_3^{2-}$ )

Mineral	1	2	3	4	5	6	7	8	9	10	11
CaO	30.33	32.00	32.13	29.65	29.51	28.94	28.87	28.51	28.87	28.61	27.00
MgO	21.26	19.74	18.23	18.15	16.52	15.26	12.66	12.24	8.58	7.88	6.22
FeO	0.07	0.89	2.53	4.25	6.43	7.22	11.70	13.96	17.78	18.60	19.83
MnO	0.06	0.11	0.25	0.89	1.37	2.44	0.91	0.63	0.81	1.30	1.99
$\text{CO}_2$	47.08	47.27	46.81	46.22	45.97	45.29	44.19	44.66	43.41	43.24	41.34
Insoluble	1.49	0.00	0.05	0.48	0.20	0.50	1.62	0.14	0.27	0.71	3.64
Total	100.29	100.01	100.00	99.64	100.00	99.65	99.95	100.14	99.72	100.34	100.02
Number of ions on basis of $2\text{CO}_3^{2-}$											
$\text{Ca}^{2+}$	1.011	1.062	1.077	1.007	1.007	1.003	1.025	1.002	1.044	1.038	1.025
$\text{Mg}^{2+}$	0.986	0.912	0.850	0.858	0.785	0.736	0.626	0.598	0.432	0.398	0.329
$\text{Fe}^{2+}$	0.002	0.023	0.066	0.113	0.171	0.195	0.324	0.383	0.502	0.527	0.588
$\text{Mn}^{2+}$	0.002	0.003	0.007	0.024	0.037	0.067	0.026	0.017	0.023	0.037	0.060
$\text{CO}_3^{2-}$	2	2	2	2	2	2	2	2	2	2	2

1 Dolomite: Blantyre, Malawi, BGS Reference Collection RC193/1 (insoluble residue is quartz).

2 Dolomite: unknown locality (a) Kings' College, London Collection.

3 Dolomite: unknown locality (b) BGS Ludlam Collection 1704/1.

4 Ferroan dolomite: Cow Green Mine, Middleton-in-Teesdale (a) BGS Ludlam Collection 31384.

5 Ferroan dolomite: Cow Green Mine, Middleton-in-Teesdale (b) BGS Ludlam Collection 31379.

6 Ankerite: Bossiney, Tintagel, Cornwall.

7 Ankerite: Erzberg, Austria (a) BGS Ludlam Collection 29916b (insoluble residue includes 1.25%  $\text{Fe}_2\text{O}_3$ ).

8 Ankerite: Nova Scotia, BGS Ludlam Collection 24428.

9 Ankerite: Bersham Colliery, Clwyd, BGS Ludlam Collection 30117.

10 Ankerite: Erzberg, Austria (b) BGS Ludlam Collection 29916a.

11 Ankerite: Erzberg, Austria (c) BGS Ludlam Collection 29915.

spectroscopy (IR) prior to chemical and thermal analyses. Chemical analyses were determined on solutions in 10% hydrochloric acid by inductively coupled plasma-atomic absorption spectroscopy (ICP-AAS).  $\text{CO}_2$  was calculated on the basis of  $\text{M}^{2+}\text{CO}_3^{2-}$ . Some samples were found to contain traces of soluble salts which severely affected the initial thermal analysis results. These salts were removed by gentle washing of the less than  $63\ \mu\text{m}$  powdered minerals with deionized water; the washed material was then dried at ambient temperature immediately prior to thermal analysis to minimize oxidation effects.

Thermogravimetric-differential thermogravimetric (TG-DTG) curves were obtained with a Stanton Redcroft TG-770 microthermobalance in flowing  $\text{CO}_2$  ( $10\ \text{ml min}^{-1}$ ); 10 mg samples were used at a heating rate of  $15^\circ\text{C min}^{-1}$ . Thermomagnetometry (TM) of the decomposition products was carried out on the same apparatus by placing small permanent magnets around the thermobalance furnace during normal TG runs (heating and cooling); Curie points were estimated from these curves.

Simultaneous DTA-evolved gas analysis (EGA) curves were produced by linking a modified DTA furnace to non-dispersive infrared  $\text{CO}_2$  and CO analysers. The system used was similar to that described by Morgan [19] but with the addition of a CO analyser. The gas analysers were calibrated initially using standard gases but calibration was checked by running standard samples of sodium bicarbonate and magnesium oxalate which decompose by known mechanisms to yield  $\text{H}_2\text{O} + \text{CO}_2$  and  $\text{CO}_2 + \text{CO}$  respectively [20,21]. The carrier gas was dry  $\text{N}_2$  (flow rate  $300\ \text{ml min}^{-1}$ ). Sample size was approximately 60 mg and a heating rate of  $15^\circ\text{C min}^{-1}$  was used. Further DTA-EGA (CO analyser) curves were obtained using  $\text{CO}_2$  as the carrier gas (flow rate  $300\ \text{ml min}^{-1}$ , nominal), 150 mg samples and a  $15^\circ\text{C min}^{-1}$  heating rate.

Continuous heating X-ray powder photographs were recorded in  $\text{CO}_2$  atmosphere for two ankerites (6, 11; Table 1). The X-ray diffraction photographs were recorded using an Enraf-Nonius Guinier-Lenne heating camera during 12-h runs over the temperature interval  $500\text{--}1000^\circ\text{C}$ .

Decomposition products were also cooled from intermediate temperatures during TG runs and identified primarily by X-ray powder photography (Debye-Scherrer camera).  $\text{Cu K}\alpha$  radiation was used with Si metal as an internal standard. Where sufficient material was available, larger amounts of intermediate products were prepared by heating samples in the DTA-EGA apparatus. These samples were then examined by XRD. However, since the DTA-EGA furnace could not be quenched as rapidly as the TG furnace, the residues may have continued to decompose to some extent during cooling.

Samples of the most ferroan ankerite (11; Table 1) heated to each of the three major TG weight loss steps in  $\text{CO}_2$  were examined by Mössbauer spectroscopy [22].

## RESULTS AND DISCUSSION

*TG-DTG curve configuration in air and CO<sub>2</sub>*

TG-DTG curves of end-member dolomite in air (Fig. 1a) show two ill-defined weight losses each corresponding to approximately half the CO<sub>2</sub> content of the mineral. As shown for DTA curves by Warne et al. [11], these weight loss reactions can be separated and better defined by conducting TG-DTG analyses in flowing CO<sub>2</sub> (Fig. 1b).

In the absence of soluble salts, the TG-DTG curves in CO<sub>2</sub> of end-member dolomite show that decomposition begins at approximately 700 °C, producing a DTG peak at about 760 °C for the first weight loss step (Fig. 2a). The TG curve then almost plateaus except for a small but perceptible and gradual weight loss up to 920 °C when the very rapid second weight loss step begins. This weight loss shows a DTG peak at about 950 °C (Fig. 2a). As the Fe<sup>2+</sup> content of dolomite increases through the series dolomite-ferroan dolomite-ankerite, another weight loss step becomes apparent on the TG curves in CO<sub>2</sub>. This step occurs between the two weight losses seen in end-member dolomite (Fig. 2b). As for dolomite, the first weight loss corresponds approximately to half the CO<sub>2</sub> content of the mineral. The first weight loss step occurs at progressively lower temperatures with increasing Fe<sup>2+</sup> content of the mineral but, as seen on DTA curves [11], the iron content bears little relationship to the temperatures of either the second or third decomposition steps.

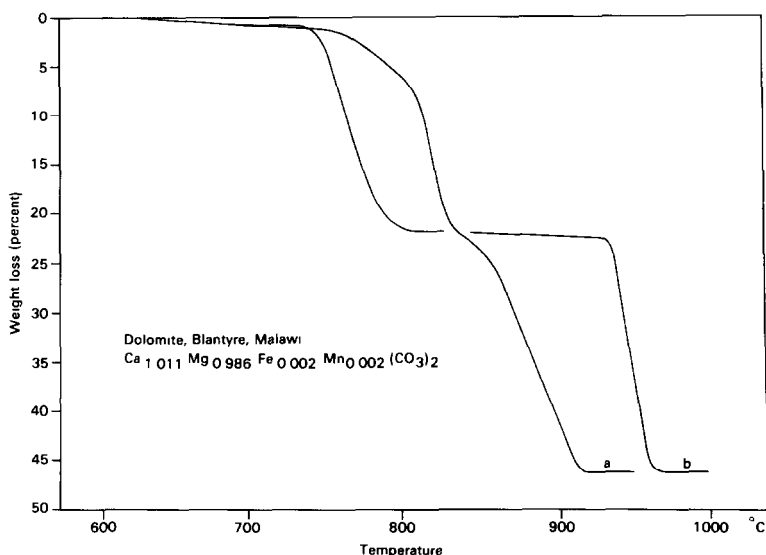


Fig. 1. Comparison of TG curves for dolomite in (a) air and (b) CO<sub>2</sub> atmospheres. Heating rate 15 °C min<sup>-1</sup>, CO<sub>2</sub> flowing 10 ml min<sup>-1</sup>, 10 mg samples.

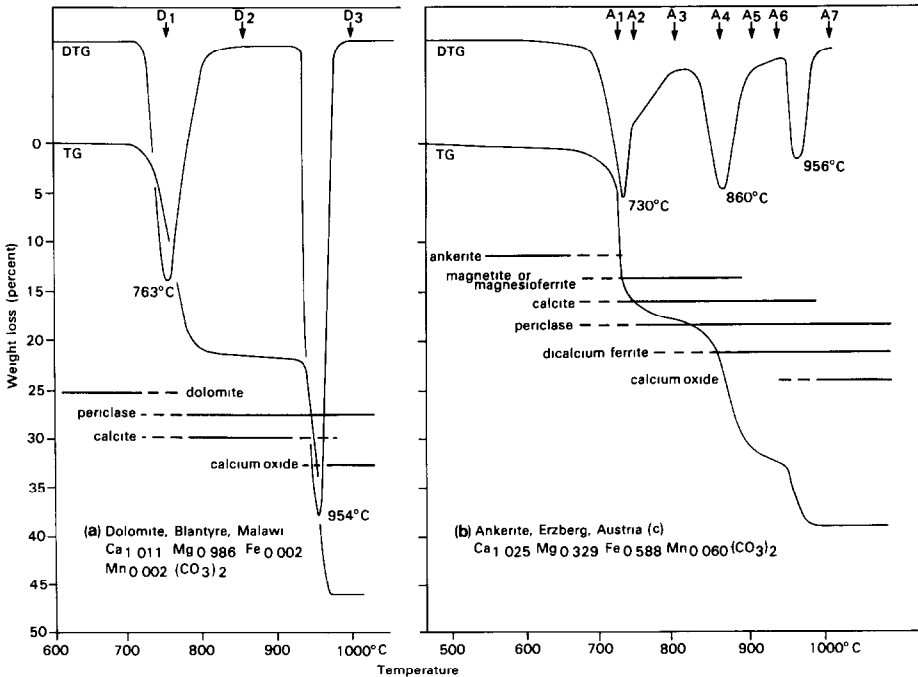


Fig. 2. TG–DTG curves for (a) dolomite and (b) ankerite in  $\text{CO}_2$  atmospheres. Residues isolated for XRD analysis indicated ( $D_1$ – $D_3$ ,  $A_1$ – $A_7$ ) together with ranges of decomposition products identified by XRD. Heating rate  $15^\circ\text{C min}^{-1}$ ,  $\text{CO}_2$  flowing  $10\text{ ml min}^{-1}$ , 10 mg samples.

### Simultaneous DTA–EGA( $\text{CO}$ , $\text{CO}_2$ ) analysis

Simultaneous DTA–EGA curves of ankerite in flowing  $\text{N}_2$  (Fig. 3) show three endothermic reactions (dolomite shows only two endothermic peaks). All three peaks correspond to the evolution of  $\text{CO}_2$  from the sample.  $\text{CO}$  is also evolved during the first two reactions, although generally  $\text{CO}$  peaks occur at slightly higher temperatures than the corresponding DTA and  $\text{CO}_2$  peaks.

In  $\text{CO}_2$  atmosphere, these reactions are better defined. Figure 4 illustrates the variation in DTA–EGA( $\text{CO}$ ) curves in  $\text{CO}_2$  atmosphere through the series dolomite–ferroan dolomite–ankerite. Dolomite (Fig. 4a) has the simplest decomposition pattern with two endothermic DTA peaks and no  $\text{CO}$  evolution.  $\text{CO}$  is evolved from the  $\text{Fe}^{2+}$ -bearing members of the series, the amount of  $\text{CO}$  evolved increasing with increasing  $\text{Fe}^{2+}$  content (Fig. 4, b–f). Also, as reported previously [11], the size of the second DTA endotherm increases with increase in  $\text{Fe}^{2+}$  content.

The  $\text{CO}$  evolution profile of the ferroan dolomites and ankerites is complex. Ferroan dolomites show three  $\text{CO}$  evolution peaks (Fig. 4, b–d), but with increasing  $\text{Fe}^{2+}$  content the pattern becomes simpler, ankerite

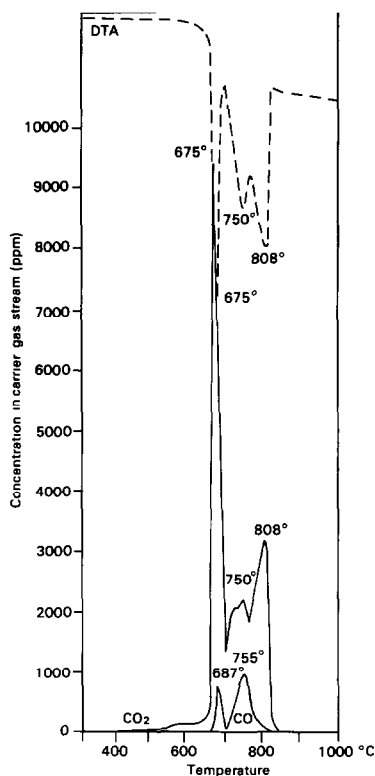


Fig. 3. Simultaneous DTA-EGA ( $\text{CO}_2$ , CO) curves of ankerite in flowing  $\text{N}_2$  atmosphere. Ankerite 11;  $\text{Ca}_{1.025}\text{Mg}_{0.329}\text{Fe}_{0.588}\text{Mn}_{0.060}(\text{CO}_3)_2$ . Heating rate  $15^\circ\text{C min}^{-1}$ ,  $\text{N}_2$  carrier gas  $300\text{ ml min}^{-1}$ , 100 mg sample.

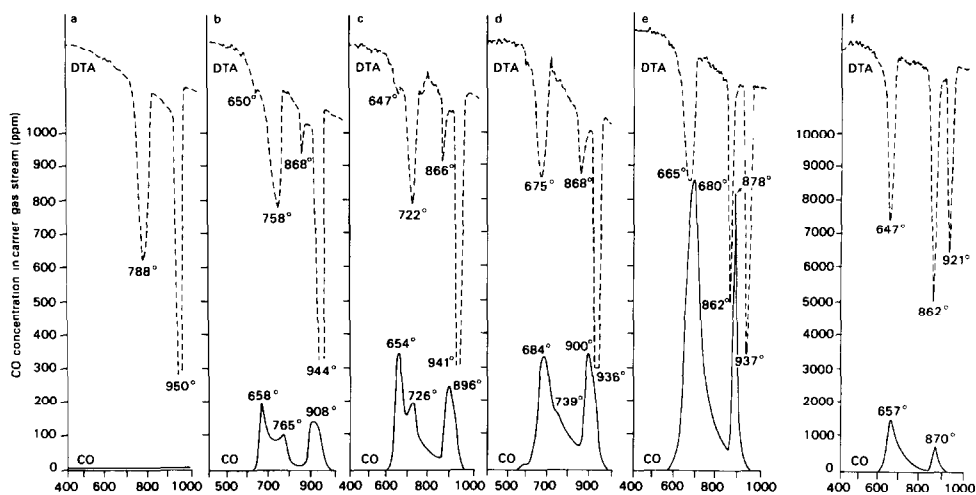


Fig. 4. Simultaneous DTA-EGA (CO) curves of dolomite, ferroan dolomite and ankerite in  $\text{CO}_2$  showing variation with iron content: a, dolomite 1,  $\text{Ca}_{1.011}\text{Mg}_{0.986}\text{Fe}_{0.002}\text{Mn}_{0.002}(\text{CO}_3)_2$ ; b, ferroan dolomite 4,  $\text{Ca}_{1.007}\text{Mg}_{0.858}\text{Fe}_{0.113}\text{Mn}_{0.024}(\text{CO}_3)_2$ ; c, ferroan dolomite 5,  $\text{Ca}_{1.007}\text{Mg}_{0.785}\text{Fe}_{0.171}\text{Mn}_{0.037}(\text{CO}_3)_2$ ; d, ankerite 6,  $\text{Ca}_{1.003}\text{Mg}_{0.736}\text{Fe}_{0.195}\text{Mn}_{0.067}(\text{CO}_3)_2$ ; e, ankerite 8,  $\text{Ca}_{1.002}\text{Mg}_{0.598}\text{Fe}_{0.383}\text{Mn}_{0.017}(\text{CO}_3)_2$ ; f, ankerite 11,  $\text{Ca}_{1.025}\text{Mg}_{0.329}\text{Fe}_{0.588}\text{Mn}_{0.060}(\text{CO}_3)_2$ . Heating rate  $15^\circ\text{C min}^{-1}$ ,  $\text{CO}_2$  carrier gas  $330\text{ ml min}^{-1}$  (nominal), 100 mg samples.

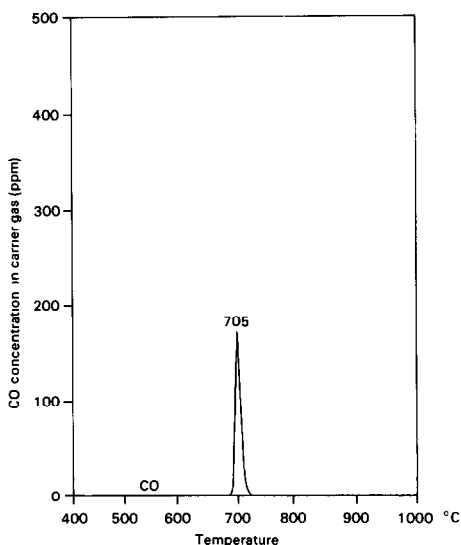


Fig. 5. EGA(CO) curve of ankerite 11 in  $\text{CO}_2$  atmosphere showing CO evolution profile of "small" sample. Heating rate  $15^\circ\text{C min}^{-1}$ ,  $\text{CO}_2$  carrier gas  $300\text{ ml min}^{-1}$  (nominal), 10 mg sample.

showing only two CO peaks (Fig. 4, e–f). At the lower Fe end of the series, the first CO evolution occurs at a significantly lower temperature (up to  $100^\circ\text{C}$ ) but the more Fe-rich members of the series have CO profiles in which the first CO peak occurs at or slightly higher than the temperature of the first DTA peak. The second CO peak ( $720\text{--}770^\circ\text{C}$ ) shows poor correlation with the DTA curve and appears to lag behind the initial DTA endotherm. As the Fe-content of the dolomite increases this second peak moves down-temperature, decreasing in size until it becomes only a shoulder to the lower temperature peak in minerals with about 20 mol%  $\text{CaFe}(\text{CO}_3)_2$  solid solution (Fig. 4d). Similarly, the third CO peak appears to lag behind the second DTA endotherm.

Sample size significantly affects both the relative amount of CO evolved and the shape of the CO evolution profile. Samples of 100–33 mg produce complex EGA profiles as seen in Fig. 4; however, only a single CO peak is seen with samples of the order of 10 mg (Fig. 5). This single peak corresponds to the temperature of the first decomposition step. Table 2 compares values of actual CO evolved with that predicted from ankerite analyses (Table 1) assuming that all  $\text{Fe}^{2+}$  is oxidized by  $\text{CO}_2$  to  $\text{Fe}^{3+}$  (eqn. (1))



Comparisons are also made for different sample sizes. The relative amount of CO evolved increases with both increasing sample size and increasing  $\text{Fe}^{2+}$  content of the ankerite. The amount of CO evolved only reaches that value predicted by eqn. (1) for relatively large samples (300 mg)



TABLE 2

Comparison of total mass of CO evolved from ankerite (measured by EGA) with calculated mass CO evolved if all  $\text{Fe}^{2+}$  is oxidized to  $\text{Fe}^{3+}$  by reduction of  $\text{CO}_2$  to CO

Sample	Sample mass (mg)	Actual CO evolved (mg)	Theoretical CO evolved (mg)	$\frac{\text{Actual CO}}{\text{Theoretical CO}}$
Ankerite 11	10	0.03	0.39	0.08
	100	2.76	3.86	0.72
	300	11.60	11.58	1.00
Ankerite 8	100	1.89	2.72	0.69
Ferroan dolomite 4	100	0.44	0.83	0.53

of the most ferroan ankerite (sample 11; Table 2). This suggests that either CO or  $\text{Fe}^{2+}$  is being oxidized by traces of  $\text{O}_2$  in the system, causing a noticeable deficit in CO measured from either low iron minerals or small samples. The source of this  $\text{O}_2$  is uncertain but may have been trapped within the sample, desorbed from the apparatus during heating, or could have diffused through the walls of the ceramic furnace tube. Another source of  $\text{O}_2$  may have been impurities in the carrier gas but attempts to remove this by passing the carrier gas over hot Cu metal did not change any of the observations above. This possible loss of CO due to oxidation must be taken into account when interpreting EGA(CO) curves.

#### *X-Ray diffraction analysis of decomposition products*

The phases identified by X-ray diffraction studies of products isolated at various stages during ankerite and dolomite decomposition are summarized in Table 3. Their distribution during thermal analysis is also illustrated in Fig. 2 (based on both "static" and "continuous" XRD observations).

Dolomite decomposition gives rise to relatively few products. The initial stage involves breakdown of the dolomite lattice with the dissociation of the  $\text{MgCO}_3$  component to yield MgO (periclase) and  $\text{CaCO}_3$  (calcite) as products. During the second decomposition stage the  $\text{CaCO}_3$  dissociates to produce CaO (lime). "Static" XRD results show that CaO may recarbonate to some extent on cooling in a  $\text{CO}_2$  atmosphere.

Ankerite and ferroan dolomite decomposition is more complex.  $\text{CaCO}_3$  (calcite) and MgO (periclase), together with a "spinel"-structure phase, form during the first stage of decomposition. X-ray data indicate either  $\text{MgFe}_2\text{O}_4$  (magnesioferrite),  $\text{Fe}_3\text{O}_4$  (magnetite) or a solid solution between these two end-members; because these two compounds have virtually identical X-ray diffraction patterns, further discrimination cannot be made by XRD. Decomposition products isolated during the early stages of this decomposition stage are poorly crystalline and give weak and broad X-ray reflections.

TABLE 3

Phases identified by XRD in products cooled from different temperatures on dolomite-ankerite TG curves (see Fig. 2)

	Temp. (°C)	Ankerite	Dolomite	CaCO <sub>3</sub>	MgO	CaO	"Spinel phase"	Ca <sub>2</sub> Fe <sub>2</sub> O <sub>5</sub>
D1	760		●	●	●			
D2	850			●	●			
D3	1000			●	●	●		
A1	730	●		●	?		?	
A2	750	○		●	○		●	
A3	800	tr		●	●		●	
A4	870			●	●		●	○
A5	900			●	●			●
A6	950			●	●			●
A7	1000			●	●			●

●, Major phase; ○, minor phase; tr, trace phase; ?, uncertain identification (lost in other phase patterns).

Powder patterns of these products compared with the following JCPDS reference patterns: ankerite (12-88), dolomite (1-78), calcite (5-586), MgO (4-829), CaO (4-777), Fe<sub>3</sub>O<sub>4</sub> (19-629),  $\gamma$ -Fe<sub>2</sub>O<sub>3</sub> (4-755, 15-615), MgFe<sub>2</sub>O<sub>4</sub> (17-464, 17-465) and Ca<sub>2</sub>Fe<sub>2</sub>O<sub>5</sub> (19-222).

Fe-bearing phases are only just detectable by XRD during this stage from ankerites with less than 20 mol% CaFe(CO<sub>3</sub>)<sub>2</sub>. During the second decomposition stage, Ca<sub>2</sub>Fe<sub>2</sub>O<sub>5</sub> (dicalcium ferrite) is formed at the expense of the "spinel" phase. The third decomposition stage involves the dissociation of any remaining CaCO<sub>3</sub> to CaO (lime). XRD spacings of dicalcium ferrite produced from Mn-rich ankerites are slightly smaller than from Mn-poor ankerites. This may indicate that Mn is preferentially incorporated into the ferrite phase during decomposition.

CaCO<sub>3</sub> produced during the first decomposition step exhibits spacings that are significantly smaller than those for pure calcite (JCPDS 5-586). With increasing temperature up to the start of the second decomposition step for both ankerite and dolomite, this difference gradually diminishes. This indicates that a small amount of MgCO<sub>3</sub> is formed in solid solution in CaCO<sub>3</sub> during the early stages of dolomite or ankerite breakdown and that this solid solution is reduced as decomposition proceeds. Comparison with XRD data in the literature for magnesian calcite [23,24] suggests that 5–10 mol% MgCO<sub>3</sub> may be present in solution in the initial CaCO<sub>3</sub> formed. These observations confirm those made earlier by Lange and Roesky [12] and Hashimoto et al. [15].

#### *Thermomagnetometry curves for ankerite decomposition products*

Thermomagnetometry (TM) curves of residues could only be realistically studied for ankerites with 20 mol% CaFe(CO<sub>3</sub>)<sub>2</sub> or more, as below this Fe

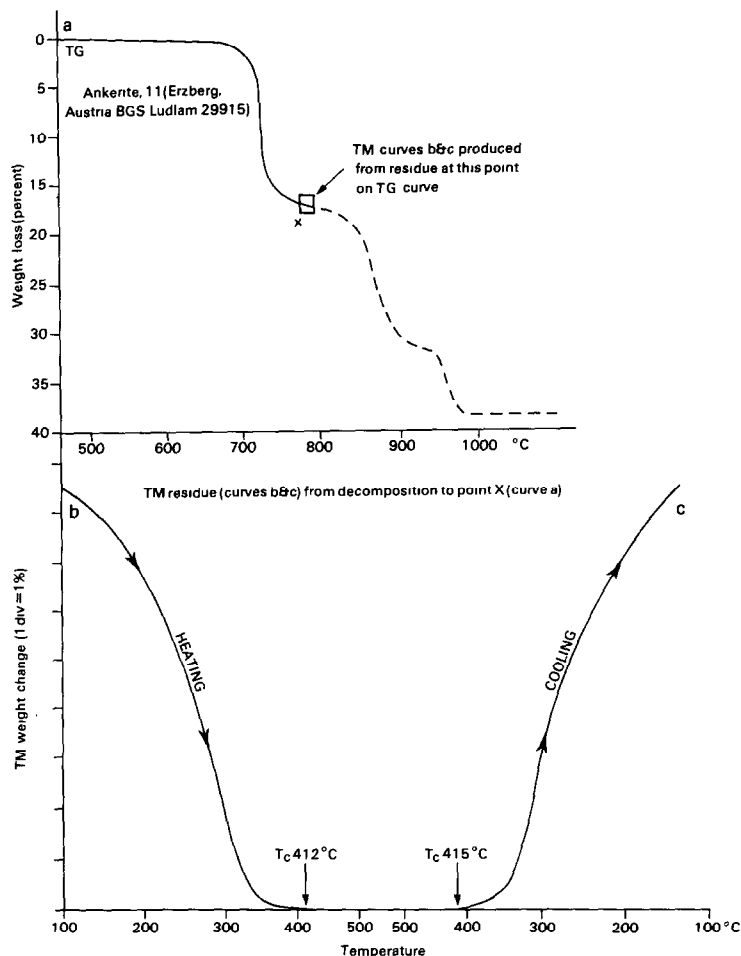


Fig. 6. TG-TM curve of ankerite 11 heated in  $\text{CO}_2$  atmosphere. TM curve produced by reheating residue (b) and cooling residue (c) isolated from point  $\times$  during TG analysis (a). Heating rate  $15^\circ\text{C min}^{-1}$ ,  $\text{CO}_2$  flowing  $10\text{ ml min}^{-1}$ , 10 mg sample.

content it was difficult to determine Curie points ( $T_c$ ) with reasonable confidence. Figure 6 illustrates a typical TM curve recorded during heating and cooling the residue produced on heating ankerite 11 (Table 1) to the end of the first reaction. The TM curve monitors the apparent weight change due to magnetic attraction as the residue is heated or cooled in a magnetic field. Figure 6b shows that the residue loses its magnetic attraction as it is heated above about  $412^\circ\text{C}$ . Similarly, on cooling the residue appears to become magnetic below  $415^\circ\text{C}$ . The temperatures at which the material loses its strong magnetic properties is taken as the Curie point ( $T_c$ ), the temperature at which ferromagnetic materials become paramagnetic [25].

Table 4 gives  $T_c$  values for the residues of three ankerites heated to the end of the first reaction. The  $T_c$  values are considerably lower than the

TABLE 4

Curie point ( $T_c$ ) of decomposition product at end of first TG weight loss in  $\text{CO}_2$  (TG decomposition at heating rate of  $15^\circ\text{C min}^{-1}$ )

Sample	$T_c$ (heating)	$T_c$ (cooling)	$T_c$ (mean)
Ankerite 11	$412^\circ\text{C} (\pm 10)$	$415 (\pm 10)$	414
Ankerite 8	$419^\circ\text{C} (\pm 15)$	$447 (\pm 15)$	433
Ankerite 6	$340^\circ\text{C} (\pm 15)$	$340 (\pm 15)$	340

published data (Table 5) for  $\text{Fe}_2\text{O}_3$  (hematite) or the spinel phases  $\text{Fe}_2\text{O}_3$  (maghemite) and  $\text{Fe}_3\text{O}_4$  (magnetite).  $T_c$  values of ankerites 11 and 8 ( $410\text{--}450^\circ\text{C}$ ) are very close to  $\text{MgFe}_2\text{O}_4$  (magnesioferrite) but the residue from ankerite 6 has a much lower  $T_c$  ( $340^\circ\text{C}$ ). If the  $\text{Mn}^{2+}$  contents of the ankerites are taken into account, then the  $T_c$  values of the residues are consistent with those of the spinels that would be expected to form in the series  $\text{MgFe}_2\text{O}_4\text{--MnFe}_2\text{O}_4$ , assuming that (i) all the  $\text{Fe}^{2+}$  is oxidized to  $\text{Fe}^{3+}$ , (ii) all the  $\text{Mn}^{2+}$  is incorporated into the spinel phase (there is no evidence to the contrary from XRD observations) and (iii) the extrapolation of  $T_c$  between  $\text{MgFe}_2\text{O}_4$  and  $\text{MnFe}_2\text{O}_4$  [26] is correct. This comparison is shown in Fig. 7 and Table 6.

Curie points estimated at various stages through the first and second TG weight losses of ankerite 11 show a gradual decrease in temperature from about  $500^\circ\text{C}$  during the early stages of the first TG step (Table 7) to  $410\text{--}415^\circ\text{C}$  at the end of this reaction. Rapid heating rates ( $50^\circ\text{C min}^{-1}$ ) produce  $T_c$ 's with higher values during this step. This would indicate that some  $\text{Fe}^{2+}$  may be initially incorporated in the spinel structure and that the  $T_c$  is tending towards that for magnetite ( $T_c = 585^\circ\text{C}$ ). During the second TG weight loss there is a rapid drop in  $T_c$  of the residue and also of the

TABLE 5

Curie points ( $T_c$ ) of various compounds (after Gallagher and Warne [26])

Compound	$T_c$ ( $^\circ\text{C}$ )
$\alpha\text{-Fe}_2\text{O}_3$	675
$\gamma\text{-Fe}_2\text{O}_3$	585
$\text{Fe}_3\text{O}_4$	585
$\text{MgFe}_2\text{O}_4$	440
$\text{MnFe}_2\text{O}_4$	300
$\text{Mn}_3\text{O}_4$	230
$\text{Mn}_{0.91}\text{Mg}_{0.09}\text{Fe}_2\text{O}_4$	313 <sup>a</sup>
$\text{Mn}_{0.40}\text{Mg}_{0.60}\text{Fe}_2\text{O}_4$	384 <sup>a</sup>
$\text{Mn}_{0.35}\text{Mg}_{0.65}\text{Fe}_2\text{O}_4$	391 <sup>a</sup>

<sup>a</sup> Values predicted for decomposition products of siderite [26].

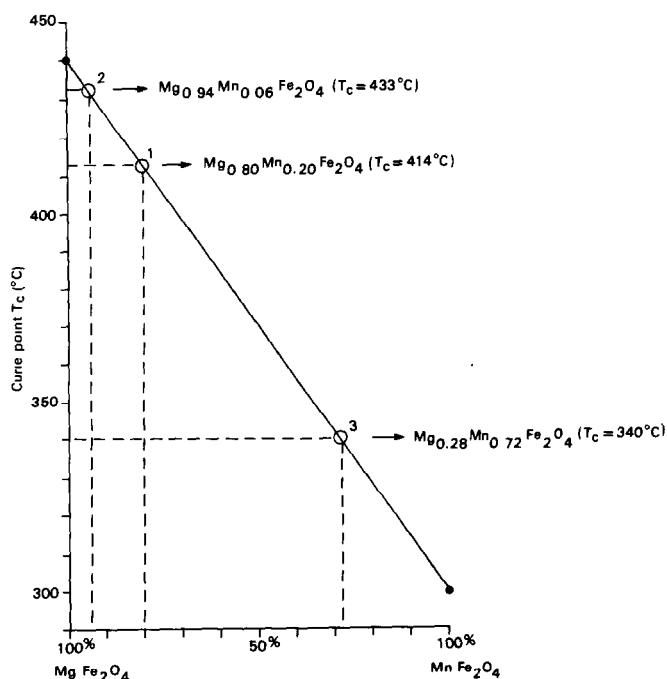


Fig. 7. Extrapolation of Curie points ( $T_c$ ) between  $T_c$  of end-member spinels in the series  $\text{MgFe}_2\text{O}_4$ – $\text{MnFe}_2\text{O}_4$  assuming linear relationship between  $T_c$  and spinel composition [21]. Also shown are compositions of spinels predicted from this extrapolation as indicated by the mean  $T_c$  of the residue of (1) ankerite 11, (2) ankerite 8, and (3) ankerite 6, after the first decomposition stage in  $\text{CO}_2$  atmosphere.

degree of magnetic attraction experienced, until the product at the end of this stage which is only feebly magnetic with an indistinct  $T_c$  of about  $220^\circ\text{C}$ .

TABLE 6

Comparison of compositions of spinel phases in the series  $\text{MgFe}_2\text{O}_3$ – $\text{MnFe}_2\text{O}_3$  predicted to form from ankerite (assuming total oxidation of  $\text{Fe}^{2+}$ ) with that estimated by measurement of Curie point ( $T_c$ ) by TG–TM

Sample	Composition predicted by eqn. (1)	Composition predicted by $T_c$
Ankerite 11 $\text{Ca}_{1.025}\text{Mg}_{0.329}\text{Mn}_{0.060}\text{Fe}_{0.588}(\text{CO}_3)_2$	$\text{Mg}_{0.80}\text{Mn}_{0.20}\text{Fe}_2\text{O}_4$	$\text{Mg}_{0.80}\text{Mn}_{0.20}\text{Fe}_2\text{O}_4$
Ankerite 8 $\text{Ca}_{1.002}\text{Mg}_{0.598}\text{Mn}_{0.017}\text{Fe}_{0.383}(\text{CO}_3)_2$	$\text{Mg}_{0.91}\text{Mn}_{0.09}\text{Fe}_2\text{O}_4$	$\text{Mg}_{0.94}\text{Mn}_{0.06}\text{Fe}_2\text{O}_4$
Ankerite 6 $\text{Ca}_{1.003}\text{Mg}_{0.736}\text{Mn}_{0.067}\text{Fe}_{0.195}(\text{CO}_3)_2$	$\text{Mg}_{0.31}\text{Mn}_{0.69}\text{Fe}_2\text{O}_4$	$\text{Mg}_{0.28}\text{Mn}_{0.72}\text{Fe}_2\text{O}_4$

TABLE 7

Curie points ( $T_c$ ) estimated from TM curves for decomposition products formed at various stages during thermal decomposition of ankerite 11 in  $\text{CO}_2$  atmosphere

TG loss (%)	$T_c$ (heating) ( $^{\circ}\text{C}$ )	$T_c$ (cooling) ( $^{\circ}\text{C}$ )	
Products produced in TG apparatus at $50^{\circ}\text{C min}^{-1}$ heating rate			
3.8	490	505	1st TG weight loss
14.8	485	490	
16.0	500	510	
17.0	360	385	2nd TG weight loss
17.8	320	317	
18.7	310	320	
20.4	277	284	
21.8	270	270	
24.4	266	266	
27.6	258	258	
32.8 <sup>a</sup>	226	215	
Product produced in TG apparatus at $15^{\circ}\text{C min}^{-1}$ heating rate to end of first weight loss			
16.5	412	415	
Product produced in TG apparatus at isothermal heating at $660^{\circ}\text{C}$ for 120 minutes			
6.0	410	410	

<sup>a</sup> Denotes product only very weakly magnetic.

### *Mössbauer spectroscopy of decomposition products*

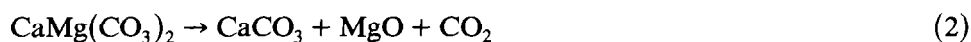
Mössbauer spectra of decomposition products are described in detail elsewhere [22] and the results are only briefly discussed here. The results generally confirm identifications made on the basis of XRD and TM. The spectra show clearly that the bulk of the iron in the unaltered ankerite (ankerite 11) is in the  $\text{Fe}^{2+}$  form and spectra are consistent with those reported in the literature for ferrous carbonates [27]. After heating to near the end of the first decomposition step on the TG curves, Mössbauer spectra indicate that all the  $\text{Fe}^{3+}$  is in a magnetically ordered structure in an oxide environment. This product is definitely not magnetite but could have a spinel-type structure. A small amount of  $\text{Fe}^{2+}$  remains but the quadrupole splitting of this  $\text{Fe}^{2+}$  is different from that in unaltered ankerite. Neither is the  $\text{Fe}^{2+}$  consistent with its being present in a magnetically ordered spinel structure. The Mössbauer spectra have been interpreted [22] as arising from a mixture of  $\text{MgFe}_2\text{O}_4$  and a small amount of unreacted  $(\text{Mg,Fe})\text{O}$ .

### DECOMPOSITION MECHANISM OF DOLOMITE-FERROAN DOLOMITE-ANKERITE SERIES IN $\text{CO}_2$

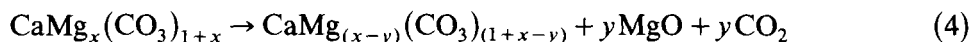
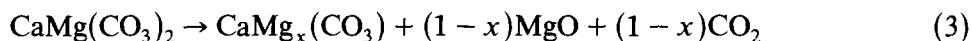
Previous studies on the thermal decomposition of dolomite in air or  $\text{CO}_2$  [12,15,28,29] have shown that dolomite dissociates in two stages. The first

stage appears to involve dissociation to  $\text{CaCO}_3$ ,  $\text{MgO}$  and  $\text{CO}_2$  and the second dissociation of  $\text{CaCO}_3$  yields  $\text{CaO}$  and  $\text{CO}_2$ . In contrast, the thermal decomposition of ankerite is more complex and it has been suggested that the first reaction of ankerite is due to decomposition of both the  $\text{FeCO}_3$  and  $\text{MgCO}_3$  components [8,12,28,31], followed by oxidation of  $\text{FeO}$ , to give  $\text{CaCO}_3$ ,  $\text{MgO}$  and  $\gamma\text{-Fe}_2\text{O}_3$  in air [8] or  $\text{CaCO}_3$  and  $\text{MgFe}_2\text{O}_4$  in both  $\text{CO}_2$  and air [28,30]. The second stage of the reaction has been attributed to the solid state reaction between  $\text{CaCO}_3$  and the iron-bearing phases to produce  $\text{CaFe}_2\text{O}_4$  [8] or  $\text{Ca}_2\text{Fe}_3\text{O}_5$  [31].

The results of this study agree in general terms with previous work [12,15] on the decomposition of the dolomite end-member of the series. The weight loss recorded by TG in  $\text{CO}_2$  for the first reaction is less than expected for the simple relationship in eqn. (2)



This must therefore be regarded as a simplistic scheme. The XRD results suggest that 5–10 mol%  $\text{MgCO}_3$  is present in solid solution within the  $\text{CaCO}_3$  produced during reaction (2).  $P_{\text{CO}_2}$ - $T$  phase equilibria published for dolomite–Mg–calcite relationships [32] indicate that at  $P_{\text{CO}_2} = 1$  atm, dolomite should decompose initially (at equilibrium) to periclase and Mg-calcite (6 mol%  $\text{MgCO}_3$  in solid solution). With increasing  $P_{\text{CO}_2}$ , more Mg-rich calcites are produced. Allowing for possibly higher  $P_{\text{CO}_2}$  produced within samples during decomposition, this is very close to the values indicated from the XRD data of dolomite decomposition products seen in this study. With increasing temperature, Mg-calcite should progressively decompose to periclase and less Mg-rich calcites [32]. This is consistent with the TG observations which indicate slight but continuous weight losses over the plateau between the first and second reaction. Equation (2) can therefore be modified as shown below

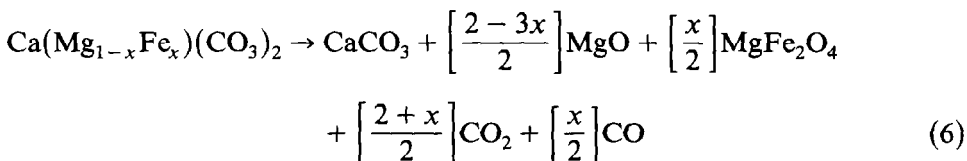


The second decomposition step can be assigned as in previous studies to the decomposition of  $\text{CaCO}_3$  (eqn. (5))



The first weight loss step in  $\text{CO}_2$  for ankerites is similarly less than expected from the combined decarbonation of the  $\text{MgCO}_3$ ,  $\text{FeCO}_3$  and  $\text{MnCO}_3$  components, even allowing for the weight gain due to oxidation of  $\text{Fe}^{2+}$ . As for dolomite, XRD evidence indicates that Mg-calcites are produced as decomposition products. Other products identified at the end of this stage also include  $\text{MgO}$  and a spinel phase in the series  $\text{MgFe}_2\text{O}_4$ – $\text{MnFe}_2\text{O}_4$ , the exact composition depending on the initial  $\text{Mn}^{2+}$  content of the ankerite. All  $\text{Mn}^{2+}$  appears to be incorporated in the spinel

phase and there is no evidence from XRD to indicate any solid solution in MgO at the end of this stage. The overall reaction can be written



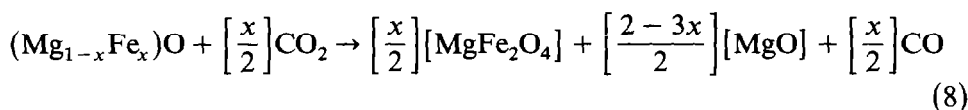
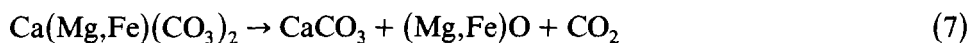
However, this is still an oversimplified scheme. Mössbauer spectra indicate the possible presence of relicts of  $\text{Fe}^{2+}$  possibly in solid solution with MgO in residues from near the end of the reaction. The  $\text{Fe}^{2+}$  is not considered to be present in the magnetically ordered spinel structure ( $\text{MgFe}_2\text{O}_4$ ). By analogy with the thermal decomposition of siderite ( $\text{FeCO}_3$ ) [26,33,34], FeO or a FeO–MgO solid solution compound would be expected to form from the  $\text{FeCO}_3$  component of ankerite as an initial product. Since ankerite decomposition in  $\text{CO}_2$  atmosphere occurs at temperatures in excess of  $600^\circ\text{C}$ , FeO would be stable and not dissociate to  $\text{Fe} + \text{Fe}_3\text{O}_4$  [33]. X-ray reflections from the MgO phase in early formed products were too indistinct to detect any line-shifts due to the possible inclusion of FeO in solid solution.

EGA showed that there were two CO-evolving reactions over this temperature interval for ferroan dolomites. These two reactions are less clearly separated in higher Fe ankerites. With increasing Fe content the higher temperature CO peak moves downscale and coalesces with the first CO peak as the Fe content increases (Fig. 4). Evolution of CO indicates the reduction of  $\text{CO}_2$  by  $\text{Fe}^{2+}$ . Previous studies on siderite decomposition [26,33,34] have shown that  $\text{Fe}^{2+}\text{Fe}_2^{3+}\text{O}_4$  (magnetite) is produced in neutral or  $\text{CO}_2$  atmospheres by the oxidation of FeO by  $\text{CO}_2$ . For ankerite, the end-product appears to be  $\text{MgFe}_2^{3+}\text{O}_4$  (magnesioferrite), in which all the Fe is in the  $\text{Fe}^{3+}$  state. Measurement of the total CO evolved during ankerite decomposition supports the conclusion that all the  $\text{Fe}^{2+}$  is oxidized to  $\text{Fe}^{3+}$  (based on measurements from relatively large samples in order to overcome the effects of oxidation due to  $\text{O}_2$  from extraneous sources). EGA of small samples shows that CO is evolved only during the first decomposition stage. TM of residues from part way through the reaction show that the initial spinel phase contains significant  $\text{Fe}^{2+}$  in solid solution as the  $T_c$  (Curie point) is intermediate between that of magnetite ( $T_c = 585^\circ\text{C}$ ) and magnesioferrite ( $T_c = 440^\circ\text{C}$ ). The  $\text{Fe}^{2+}$  would appear to oxidize progressively during the reaction to give a decomposition product with a  $T_c$  close to magnesioferrite (Mn-rich ankerites give products with even lower  $T_c$  values). The second EGA (CO) peak of ferroan dolomite may therefore represent oxidation of the  $\text{Fe}^{2+}$ -bearing spinel as a result of reaction with  $\text{CO}_2$ . Alternatively this may represent direct oxidation of (Mg,Fe)O to  $\text{MgFe}_2\text{O}_4$  by  $\text{CO}_2$ . The reason why the second CO peak is at a significantly higher

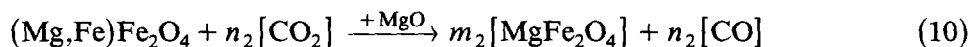
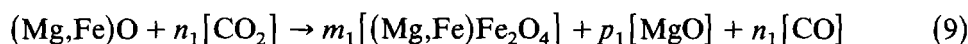


temperature in the more magnesian ankerites is unclear but possibly decomposition products with a higher Mg content may be more stable.

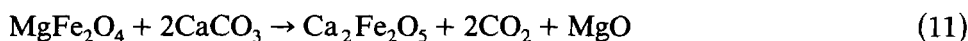
The actual path of decomposition appears to be highly dependent on experimental conditions. TM curves suggest that rapid heating rates produce an intermediate spinel phase with a significant  $\text{Fe}^{2+}$  content, whereas decomposition at slower heating rates or under isothermal conditions produces  $\text{MgFe}_2\text{O}_4$  without any indication of a  $\text{Fe}^{2+}$ -rich spinel precursor. Rapid heating rates lead to rapid decomposition during which a significantly high  $P_{\text{CO}}$  may build up within the sample thereby buffering the oxidation and temporarily stabilizing the more  $\text{Fe}^{2+}$ -rich phases. The decomposition of ankerite during the first stage may be expressed as in eqns. (7) and (8)



Equation (8) could be represented by the following two consecutive reactions



The second decomposition step for ankerite results in the formation of  $\text{Ca}_2\text{Fe}_2\text{O}_5$  and the loss of  $\text{MgFe}_2\text{O}_4$ . This implies that a solid state reaction between  $\text{CaCO}_3$  and  $\text{MgFe}_2\text{O}_4$  must occur with the liberation of  $\text{CO}_2$  and  $\text{MgO}$ . The small amount of CO evolved during this reaction from relatively large samples (> 100 mg) of ankerite is inferred to represent the oxidation of any unreacted  $(\text{Mg},\text{Fe})\text{O}$  produced during the first decomposition step. As the XRD spacings of dicalcium ferrite produced from Mn-rich ankerites are smaller than those of ferrites from the Mn-poor minerals, it is concluded that this phase acts as a sink for Mn. There is no evidence to support the incorporation of Mn in  $\text{MgO}$ . Thermomagnetometry shows that during decomposition  $T_c$  gradually decreases from  $415^\circ\text{C}$  (magnesioferrite) to about  $220^\circ\text{C}$ ; at the same time the material becomes only feebly magnetic. The reason for this behaviour is unclear, but may be due to migration of  $\text{Ca}^{2+}$  into the magnesioferrite lattice during the early stages of the solid state reaction.  $\text{Ca}_2\text{Fe}_2\text{O}_5$  is known to be only weakly ferromagnetic [35]. The second decomposition step is outlined in eqn. (11)



The final decomposition step of ankerite is similar to the second decomposition step of dolomite, representing the dissociation of any remaining  $\text{CaCO}_3$  to  $\text{CaO}$  and  $\text{CO}_2$  (eqn. (5)).

## CONCLUSIONS

The thermal decomposition of dolomite and ferroan dolomite–ankerite in a  $\text{CO}_2$  atmosphere proceeds in two and three overall stages respectively. The first stage initially involves the breakdown of the double carbonate structure and the dissociation of the Mg- and Fe-carbonate components to  $(\text{Mg,Fe})\text{O}$  (periclase–wustite solid solution) and  $\text{CO}_2$ . In ankerites and ferroan dolomites, the  $(\text{Mg,Fe})\text{O}$  produced is rapidly oxidized by  $\text{CO}_2$  (either from the ambient furnace atmosphere or self-generated atmosphere) resulting in the formation of  $\text{MgFe}_2\text{O}_4$  (magnesioferrite) and  $\text{CO}$ . Depending on experimental conditions, a  $\text{Fe}^{2+}$ -rich spinel,  $(\text{Mg,Fe})\text{Fe}_2\text{O}_4$  (magnesioferrite–magnetite solid solution), may be temporarily stabilized by the buffering effect of self-generated  $\text{CO}$  as an intermediate product. The weight loss during this reaction is less than expected for  $\text{CO}_2$  evolution from Mg- and Fe-carbonate components even allowing for the effect of oxidation of  $\text{Fe}^{2+}$ . This is due to the incorporation of some of the Mg in solid solution in  $\text{CaCO}_3$  as a reaction product. The Mg content of the  $\text{CaCO}_3$  gradually decreases with increasing temperature with the liberation of  $\text{MgO}$  and  $\text{CO}_2$ .  $\text{Mn}^{2+}$  is incorporated in the spinel phase.

The second decomposition reaction of ankerites and ferroan dolomites involves a solid state reaction between  $\text{CaCO}_3$  and the  $\text{MgFe}_2\text{O}_4$  produced during the first stage to produce  $\text{Ca}_2\text{Fe}_2\text{O}_5$  (dicalcium ferrite),  $\text{MgO}$  (periclase) and  $\text{CO}_2$ . Any  $\text{Mn}^{2+}$  is incorporated in the ferrite phase. Finally, the remaining excess  $\text{CaCO}_3$  decomposes to  $\text{CaO}$  (lime) and  $\text{CO}_2$  during the second and third stage of the decomposition of dolomite and ankerite respectively.

## ACKNOWLEDGEMENTS

This work was carried out whilst AEM was in receipt of a CASE research award from the Natural Environment Research Council (NERC).

This paper is published by permission of the Director, British Geological Survey (NERC).

## REFERENCES

- 1 M.H. Hey, *An Index of Mineral Species and Varieties*, British Museum, London, 1955.
- 2 W.A. Deer, R.A. Howie and J. Zussman, *Rock Forming Minerals*, Vol 5: Non-Silicates, Longmans, London, 1962.
- 3 R.J. Reeder, in R.J. Reeder (Ed.), *Carbonates: Mineralogy and Chemistry*, Reviews in Mineralogy II, Mineralogical Society of America, Washington, DC, 1983, pp. 1–48.
- 4 H.R. Shaw, *Bull. Geol. Soc. Am.*, 70 (1959) 1674.
- 5 M.P. Jones and R.J. Fullard, *Trans. Inst. Min. Metall.*, Section C75 (1966) 127.

- 6 R.A. Howie and F.M. Broadhurst, *Am. Mineral.*, 43 (1958) 1210.
- 7 J.R. Goldsmith, D.L. Graf, J. Withers and D.A. Northrop, *J. Geol.*, 70 (1962) 659.
- 8 J.L. Kulp, P. Kent and P.F. Kerr, *Am. Mineral.*, 36 (1951) 643.
- 9 S.St.J. Warne, *J. Sediment. Petrol.*, 32 (1962) 29.
- 10 V.C. Farmer and S.St.J. Warne, *Am. Mineral.*, 63 (1978) 779.
- 11 S.St.J. Warne, D.J. Morgan and A.E. Milodowski, *Thermochim. Acta*, 51 (1981) 105.
- 12 P.A. Lange and W. Roesky, *Ber. Dtsch. Keram. Ges.*, 41 (1964) 497.
- 13 J.W. Smith, *Thermal Analysis*, 3, Proc. 3rd ICTA (Davos) (1971) 605.
- 14 E.A. Powell and A.W. Searcy, *J. Am. Ceram. Soc.*, 61 (1978) 216.
- 15 H. Hashimoto, E. Komaki, F. Hayashi and T. Uematsu, *Solid State Chem.*, 33 (1980) 181.
- 16 K. Iwafuchi, C. Watanabe and R. Otsuka, *Thermochim. Acta*, 66 (1983) 105.
- 17 R. Otsuka, *Thermochim. Acta*, 100 (1986) 69.
- 18 A.E. Milodowski, D.J. Morgan and S.St.J. Warne, in preparation.
- 19 D.J. Morgan, *J. Therm. Anal.*, 12 (1977) 245.
- 20 E.M. Barrall and L.B. Rogers, *J. Inorg. Nucl. Chem.*, 28 (1966) 41.
- 21 D. Dollimore, in R.C. Mackenzie (Ed.), *Differential Thermal Analysis*, Vol. 1, Academic Press, London, 1970, p. 395.
- 22 A.E. Milodowski, B.A. Goodman and D.J. Morgan, *Mineral. Mag.*, 53 (1989), in press.
- 23 J.R. Goldsmith, D.L. Graf and O.I. Joensuu, *Geochim. Cosmochim. Acta*, 7 (1955) 212.
- 24 F.T. Mackenzie, W.D. Bischoff, F.C. Bishop, L. Loijens, J. Schoonmaker and R. Wollast, in R.J. Reeder (Ed.), *Carbonates: Mineralogy and Chemistry*, *Reviews in Mineralogy II*, Mineralogical Society of America, 1983, p. 97.
- 25 L.N. Mulay, *Anal. Chem.*, 34 (1962) 343.
- 26 P.K. Gallagher and S.St.J. Warne, *Thermochim. Acta*, 43 (1981) 253.
- 27 J.G. Stevens, H. Pollak, L. Zhe, R.M. White and J.L. Gibson, *Mineral Data*, Mössbauer Effect Data Center, Univ. N. Carolina, Asheville, NC, 1983.
- 28 D.R. Dasgupta, *Mineral. Mag.*, 36 (1967) 138.
- 29 R.A.W. Haul and H. Heystek, *Am. Mineral.*, 37 (1952) 166.
- 30 L.A. Conradi and T. Holth, *Proc. Int. Symp. React. Solids (Gothenburg)*, 1 (1954) 441.
- 31 D.R. Dasgupta, *Mineral. Mag.*, 35 (1965) 634.
- 32 D.L. Graf and J.R. Goldsmith, *Geochim. Cosmochim. Acta*, 7 (1955) 109.
- 33 H.E. Powell, Report of Investigations 6643, Bureau of Mines, U.S. Dept of Interior, 1965.
- 34 P.K. Gallagher, K.W. West and S.St.J. Warne, *Thermochim. Acta*, 50 (1981) 41.
- 35 S. Geller, R.W. Grant and U. Gonser, in H. Reiss (Ed.), *Progress in Solid State Chemistry*, 5, Pergamon, New York, 1971, p. 1.